Revisit to the theoretical analysis of a classical piezoelectric cantilever energy harvester

Maoying Zhou[1] Yuhong Zhao[2]

[1] Hangzhou Dianzi University
[2] Zhejiang University

December 5, 2019

Abstract

In this paper, we investigate the classical problem for a piezoelectric cantilever energy harvester. Theoretical solution to the problem is derived and compared to the solution by other authors. Asymptotic expansions of the solution is explored in the hope of finding a plausible approximation of the problem. Dependence of the output measures upon electromechanical coupling factor is therefore studies. Some advice are provided for the design of piezoelectric energy harvester.

1 Outline of the paper

The outline of the paper should be as follows:

- To obtain the closed form solution of the CPEH problem using the harmonic balance method
- Analyze the dependence of relative displacement function $u(z;\delta)$
- Tackling the dependence of output index χ_p and output measures $\tilde{V}_p$, $\tilde{I}_p$, and $\tilde{P}_p$ upon the electromechanical coupling factor δ and base excitation frequency f_b
- Derive the asymptotic expansion of the CPEH problem for the displacement function $u(z;\delta)$ and the output index χ_p
- Explore the approximation error of the asymptotic expansion and provide some clues to improve the performance

2 Introduction

The soaring development of wireless sensor networks (WSNs) and Internet of Things (IoTs) in the past decades has intrigued the research into sustainable and renewable energy sources for low-power electronics. The primary research goal is to partially or even fully replace currently used battery power or utility wall power, which are generally expensive, inconvenient, and sometimes impossible. To this end, much attention has been paid to energy harvesters, which convert the available energy in the ambient environment into usable electricity. A number of principles, mechanisms, and implementations of energy harvesters have been put forward since their first appearance in the 1990s, [1, 2, 3, 4] among which piezoelectric vibration energy harvesters (PVEHs) have gained the most widespread research popularity.

PVEHs are typically composite structures made up of some piezoelectric elements and vibration transduction mechanisms. They are generally attached to the host structures and undergo forced vibration. With the help of the vibration transduction mechanisms, the piezoelectric elements are excited in the desired vibration modes and generate electrical outputs due to direct piezoelectric effect. A majority of PVEHs work in resonance, in the sense that the maximum output power for an externally connected pure resistance is achieved when the base excitation frequency matches that of the PVEH. [5] To understand the operation principles and guide the performance optimization, researchers have proposed different mathematical models for PVEHs.

A most direct and simple approach is to use the single-degree-of-freedom (SDOF) approximation, in which the electrical domain and the mechanical domain are using SDOF resonator models respectively. Besides, the electromechanical coupling between these two domains is represented by a constant coefficient. [5, 6] This lumped-parameter model provides fruitful insights into the mechanism and dynamics behind the energy harvesting process and has been employed in the performance improvement and optimization of PVEHs. [7, 8] However, it has been shown that this model only applies to one vibration mode and exhibits considerable inaccuracy in some circumstances. [9]

A different yet improved approach is to resort to the Rayleigh-Ritz method. In this approach, electromechanical model of the PVEHs in the variational form is established based on the generalized Hamilton's principle, [10] which is then discretized to a finite-dimension matrix-form state space model using the Rayleigh-Ritz method. [11] This approach can easily be modified to admit finite element analysis and be appropriate for numerical computation. Although experimentally validated and theoretically refined, [12, 13, 14, 15] this kind of method does not reflect the resonance phenomenon and the related modal expansions.

To address the issues, a formal expansion method is developed based on the theory of functional analysis. [16] Mechanical part of the PVEH is modeled using a partial differential equation with the help of Euler-Bernoulli assumptions, while the electrical part is described with an ordinary differential equation provided that a pure resistive load is connected to the PVEH. [17] Using the eigenfunctions of a cantilever beam as the basis functions, the derived system of equations is formally expanded to obtain an infinite series of sub-systems of ordinary differential equations. This method has been validated and successfully applied to PVEHs with end mass [18], to optimize the electrode coverage [19] and some other circumstances. However, it includes infinite terms of expansion and inevitably suffers from the truncation error during numerical calculation. Besides, the basis functions adopted in the above method do not take into account the piezoelectric effect and therefore fails to capture the accurate mode shape of the PVEH theoretically.

Here in this contribution, we focus on an exact analytical model classical PVEHs. Based on the Euler-Bernoulli beam model and the linear piezoelectric relations, electromechanical model of the energy harvester is established, and then converted to a boundary value problem of ordinary differential equations using the harmonic balance method. Closed-form solution of the relative displacement function of the cantilever beam as well as the output performance measures is analyzed and numerically investigated. Asymptotic expansions of the relative displacement function are calculated to obtain approximate expressions for the output index and the related output performance measures. Tips are then provided in terms of the structure design and performance optimization of piezoelectric energy harvesters.

3 Summary of the interested equations

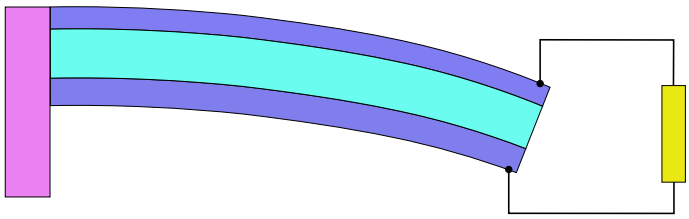

Figure 1: Schematic diagram of a typical PVEH.

The dynamic equations for a typical piezoelectric composite cantilever beam is

$$B_p \frac{\partial^4 w(x,t)}{\partial x^4} + m_p \frac{\partial^2 w(x,t)}{\partial t^2} = 0, \tag{1}$$

where B_p is the equivalent bending stiffness and m_p is the line mass density of the piezoelectric cantilever beam. If the piezoelectric elements attached to the cantilever beam is connected to an external electrical load R_l, we have

$$\frac{dQ_p(t)}{dt} + \frac{V_p(t)}{R_l} = 0. \tag{2}$$

For the underlying physics, we have the following constitutive equations

$$\begin{aligned} M_p(x,t) &= B_p \frac{\partial^2 w(x,t)}{\partial x^2} - e_p V_p(t), \\ q_p(x,t) &= e_p \frac{\partial^2 w(x,t)}{\partial x^2} + \varepsilon_p V_p(t), \end{aligned} \tag{3}$$

or equivalently,

$$\begin{cases} M_p(x,t) = B_p \dfrac{\partial^2 w(x,t)}{\partial x^2} - e_p V_p(t), \\ Q_p(x,t) = e_p \left[\dfrac{\partial w(x,t)}{\partial x} \right] \Big|_0^{l_p} + C_p V_p(t). \end{cases} \tag{4}$$

One end of the cantilever beam is fixed while the other end is free. So the boundary conditions are

$$\begin{cases} w(0,t) = w_b(t), \\ \dfrac{\partial w(0,t)}{\partial x} = 0, \end{cases} \tag{5}$$

and

$$\begin{cases} M_p(l_p,t) = B_p \dfrac{\partial^2 w(l_p,t)}{\partial x^2} - e_p V_p(t) = 0, \\ N_p(l_p,t) = \dfrac{\partial M_p(l_p,t)}{\partial x} = B_p \dfrac{\partial^3 w(l_p,t)}{\partial x^3} = 0. \end{cases} \tag{6}$$

4 Theoretical solution to the problem

In the classical energy harvesting applications, the cantilever beam is subject to a periodical base excitation $w_b(t)$. Thus the dynamic response of the cantilever beam is decomposed as

$$w(x,t) = w_b(t) + w_{rel}(x,t), \tag{7}$$

where $w_{rel}(x,t)$ is the relative displacement function of the cantilever beam. In this way, the system is converted into

$$B_p \frac{\partial^4 w_{rel}(x,t)}{\partial x^4} + m_p \frac{\partial^2 w_{rel}(x,t)}{\partial t^2} = -m_p \frac{\partial^2 w_b(t)}{\partial t^2}, \tag{8}$$

$$e_p \left[\frac{\partial^2 w_{rel}(x,t)}{\partial x \partial t} \right] \Big|_0^{l_p} + C_p \frac{dV_p(t)}{dt} + \frac{V_p(t)}{R_l} = 0. \tag{9}$$

$$\begin{cases} w_{rel}(0,t) = 0, \\ \dfrac{\partial w_{rel}(0,t)}{\partial x} = 0, \end{cases} \tag{10}$$

and

$$\begin{cases} B_p \dfrac{\partial^2 w_{rel}(l_p,t)}{\partial x^2} - e_p V_p(t) = 0, \\ \dfrac{\partial^3 w_{rel}(l_p,t)}{\partial x^3} = 0. \end{cases} \tag{11}$$

Considering a sinusoidal base excitation

$$w_b(t) = \eta_b e^{j\sigma_b t} \tag{12}$$

where ξ_b is usually a real vibration amplitude, the steady state solution for the above system can be reasonably set as

$$w_{rel}(x,t) = \eta_{rel}(x) e^{j\sigma_b t}, \quad V_p(t) = \tilde{V}_p e^{j\sigma_b t}, \tag{13}$$

where $\eta_{rel}(x)$ and $\tilde{V}_p$ are complex amplitudes. Then the above system is again simplified as

$$B_p \frac{\partial^4 \eta_{rel}(x)}{\partial x^4} - m_p \sigma_b^2 \eta_{rel}(x) = m_p \sigma_b^2 \eta_b, \tag{14}$$

$$\begin{cases} \eta_{rel}(0) = 0, \\ \dfrac{\partial \eta_{rel}(0)}{\partial x} = 0, \end{cases} \tag{15}$$

and

$$\begin{cases} B_p \dfrac{\partial^2 \eta_{rel}(l_p)}{\partial x^2} + \dfrac{j\sigma_b R_l}{1+j\sigma_b C_p R_l} e_p^2 \dfrac{\partial \eta_{rel}(l_p)}{\partial x} = 0, \\ \dfrac{\partial^3 \eta_{rel}(l_p)}{\partial x^3} = 0. \end{cases} \tag{16}$$

Note that here we assume a sinusoidal steady state response, which is not actually validated theoretically.

Obviously we can have the following dimensionless scheme:

$$\eta_{rel} \sim u\eta_b, \quad x \sim z l_p \tag{17}$$

and therefore the following dimensionless parameters

$$\sigma = \sigma_b \sqrt{\frac{m_p l_p^4}{B_p}}, \quad \beta = R_l C_p \sqrt{\frac{B_p}{m_p l_p^4}}, \quad \delta = \frac{e_p^2 l_p}{C_p B_p}. \tag{18}$$

Now, we reach the following dimensionless system of boundary value problem

$$\begin{cases} u'''' - \sigma^2 u = \sigma^2, \\ u(0) = 0, \\ u'(0) = 0, \\ u''(1) + \dfrac{j\beta\sigma}{1+j\beta\sigma}\delta u'(1) = 0, \\ u'''(1) = 0, \end{cases} \tag{19}$$

where the prime denotes the derivative with respect to z. The analytical solution to this problem can be formulated as

$$u(z;\delta) = A_\delta \cos\sqrt{\sigma}z + B_\delta \sin\sqrt{\sigma}z + C_\delta \cosh\sqrt{\sigma}z + D_\delta \sinh\sqrt{\sigma}z - 1 \tag{20}$$

and hence

$$\begin{aligned} u'(z;\delta) &= \sigma^{1/2}\left(-A_\delta \sin\sqrt{\sigma}z + B_\delta \cos\sqrt{\sigma}z + C_\delta \sinh\sqrt{\sigma}z + D_\delta \cosh\sqrt{\sigma}z\right), \\ u''(z;\delta) &= \sigma\left(-A_\delta \cos\sqrt{\sigma}z - B_\delta \sin\sqrt{\sigma}z + C_\delta \cosh\sqrt{\sigma}z + D_\delta \sinh\sqrt{\sigma}z\right), \\ u'''(z;\delta) &= \sigma^{3/2}\left(A_\delta \sin\sqrt{\sigma}z - B_\delta \cos\sqrt{\sigma}z + C_\delta \sinh\sqrt{\sigma}z + D_\delta \cosh\sqrt{\sigma}z\right). \end{aligned} \tag{21}$$

The coefficients A_δ, B_δ, C_δ, and D_δ are then subject to the following linear system of equations:

$$\begin{cases} A_\delta + C_\delta = 1, \\ B_\delta + D_\delta = 0, \\ \left(-A_\delta \cos\sqrt{\sigma} - B_\delta \sin\sqrt{\sigma} + C_\delta \cosh\sqrt{\sigma} + D_\delta \sinh\sqrt{\sigma}\right) + \\ \dfrac{j\beta\sqrt{\sigma}}{j\sigma\beta+1}\delta\left(-A_\delta \sin\sqrt{\sigma} + B_\delta \cos\sqrt{\sigma} + C_\delta \sinh\sqrt{\sigma} + D_\delta \cosh\sqrt{\sigma}\right) = 0, \\ A_\delta \sin\sqrt{\sigma} - B_\delta \cos\sqrt{\sigma} + C_\delta \sinh\sqrt{\sigma} + D_\delta \cosh\sqrt{\sigma} = 0. \end{cases} \tag{22}$$

Analytically, we can directly obtain the solution to this problem as

$$\begin{cases} A_\delta = \dfrac{1 + \cos\sqrt{\sigma}\cosh\sqrt{\sigma} - \sin\sqrt{\sigma}\sinh\sqrt{\sigma} + \frac{2j\beta\sqrt{\sigma}}{1+j\beta\sigma}\delta\left(\cos\sqrt{\sigma}\sinh\sqrt{\sigma}\right)}{2\left[1 + \cos\sqrt{\sigma}\cosh\sqrt{\sigma} + \frac{j\beta\sqrt{\sigma}}{1+j\beta\sigma}\delta\left(\cos\sqrt{\sigma}\sinh\sqrt{\sigma} + \sin\sqrt{\sigma}\cosh\sqrt{\sigma}\right)\right]}, \\ B_\delta = \dfrac{\cos\sqrt{\sigma}\sinh\sqrt{\sigma} + \sin\sqrt{\sigma}\cosh\sqrt{\sigma} + \frac{2j\beta\sqrt{\sigma}}{1+j\beta\sigma}\delta\left(\sin\sqrt{\sigma}\sinh\sqrt{\sigma}\right)}{2\left[1 + \cos\sqrt{\sigma}\cosh\sqrt{\sigma} + \frac{j\beta\sqrt{\sigma}}{1+j\beta\sigma}\delta\left(\cos\sqrt{\sigma}\sinh\sqrt{\sigma} + \sin\sqrt{\sigma}\cosh\sqrt{\sigma}\right)\right]}, \\ C_\delta = \dfrac{1 + \cos\sqrt{\sigma}\cosh\sqrt{\sigma} + \sin\sqrt{\sigma}\sinh\sqrt{\sigma} + \frac{2j\beta\sqrt{\sigma}}{1+j\beta\sigma}\delta\left(\sin\sqrt{\sigma}\cosh\sqrt{\sigma}\right)}{2\left[1 + \cos\sqrt{\sigma}\cosh\sqrt{\sigma} + \frac{j\beta\sqrt{\sigma}}{1+j\beta\sigma}\delta\left(\cos\sqrt{\sigma}\sinh\sqrt{\sigma} + \sin\sqrt{\sigma}\cosh\sqrt{\sigma}\right)\right]}, \\ D_\delta = \dfrac{-\cos\sqrt{\sigma}\sinh\sqrt{\sigma} - \sin\sqrt{\sigma}\cosh\sqrt{\sigma} - \frac{2j\beta\sqrt{\sigma}}{1+j\beta\sigma}\delta\left(\sin\sqrt{\sigma}\sinh\sqrt{\sigma}\right)}{2\left[1 + \cos\sqrt{\sigma}\cosh\sqrt{\sigma} + \frac{j\beta\sqrt{\sigma}}{1+j\beta\sigma}\delta\left(\cos\sqrt{\sigma}\sinh\sqrt{\sigma} + \sin\sqrt{\sigma}\cosh\sqrt{\sigma}\right)\right]}. \end{cases} \tag{23}$$

Firstly, to validate the closed form solution $u(z;\delta)$, we calculate the corresponding normalized output voltage $|\tilde{V}_p/(\sigma_b^2\xi_b)|$ and plot the results with respect to the base excitation frequency fr at different externally connected resistance R_l. The results are shown in Figure 2. According to the results, our calculations show a good agreement with those presented in the reference. [17]. Thus we have validated the model and the results and made our preparations for future analysis. It should be noted that, out results show an obvious difference from those in the literature [17] near the resonant frequencies. This could explained as follows. In our numerical calculations, the frequency range can be chosen to be as small as possible. A finer calculation grid leads to a sharper resonant peak. Another point to be noted is that at the resonant peak, the output voltage should arrive at its maximum and its derivative with respect to fr should be zero and the second order derivative should be infinity. In this way, a small discrepancy of the frequency from the resonant frequency leads to a large change in the normalized output voltage.

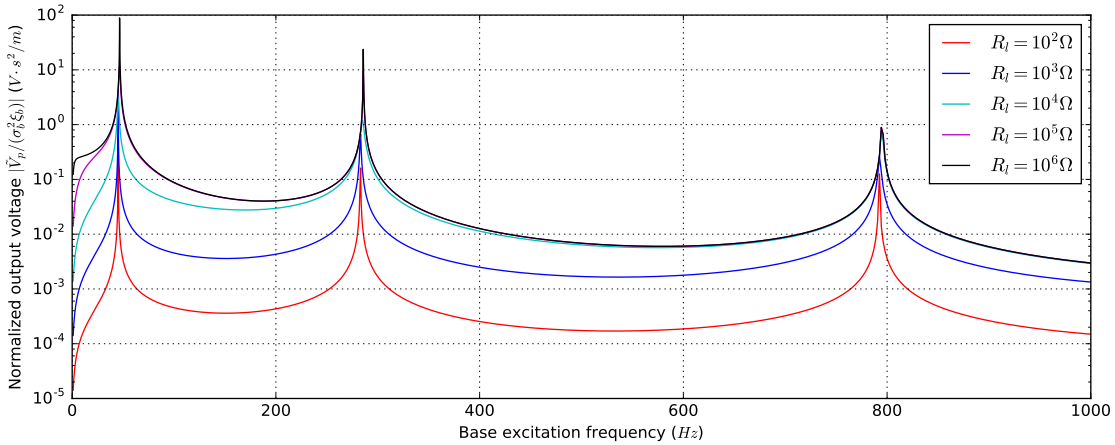

Figure 2: Validation calculation of the normalized output voltage versus base excitation frequency for a unimorph piezoelectric cantilever energy harvester based on the data from [17].

Secondly, according to equations (20) and (23), the dimensionless displacement amplitude function $u(z)$ is totally determined by the three dimensionless parameters σ, β, and δ introduced before. Among the dimensionless parameters, σ is the dimensionless base excitation frequency, β is the dimensionless electrical resonant frequency, and δ is the dimensionless electromechanical coupling strength for the structure. As σ and β is determined by the base excitation and externally connected circuit respectively, only the parameter δ is fully determined by the structure itself. Hence we would like to investigate the influence of parameter δ upon the solution displacement function $u(z)$. By taking different values of δ , we calculate the displacement amplitude function $u(z)$ and plot the results in Figure 3.

It is shown in Figure 3, the parameter δ changes the function $u(z)$ through the change of the third boundary condition (to be inserted). When δ is zero, i.e., no electromechanical coupling is present, the system degenerates to the classical elastic cantilever beam problem, whose solution is a real function. That is to say, the phase of $u(z)$ is a constant across the whole beam (in the range of $0 \le z \le 1$). Analytical expressions for the coefficients are

$$\begin{cases} A_\varnothing = \dfrac{1+\cos\sqrt{\sigma}\cosh\sqrt{\sigma}-\sin\sqrt{\sigma}\sinh\sqrt{\sigma}}{2\left[1+\cos\sqrt{\sigma}\cosh\sqrt{\sigma}\right]}, \\ B_\varnothing = \dfrac{\cos\sqrt{\sigma}\sinh\sqrt{\sigma}+\sin\sqrt{\sigma}\cosh\sqrt{\sigma}}{2\left[1+\cos\sqrt{\sigma}\cosh\sqrt{\sigma}\right]}, \\ C_\varnothing = \dfrac{1+\cos\sqrt{\sigma}\cosh\sqrt{\sigma}+\sin\sqrt{\sigma}\sinh\sqrt{\sigma}}{2\left[1+\cos\sqrt{\sigma}\cosh\sqrt{\sigma}\right]}, \\ D_\varnothing = \dfrac{-\cos\sqrt{\sigma}\sinh\sqrt{\sigma}-\sin\sqrt{\sigma}\cosh\sqrt{\sigma}}{2\left[1+\cos\sqrt{\sigma}\cosh\sqrt{\sigma}\right]}. \end{cases} \tag{24}$$

and the resulting dimensionless displacement function $u_\varnothing(z)$ is represented as

$$u_\varnothing(z) = A_\varnothing\cos\sqrt{\sigma}z + B_\varnothing\sin\sqrt{\sigma}z + C_\varnothing\cosh\sqrt{\sigma}z + D_\varnothing\sinh\sqrt{\sigma}z - 1. \tag{25}$$

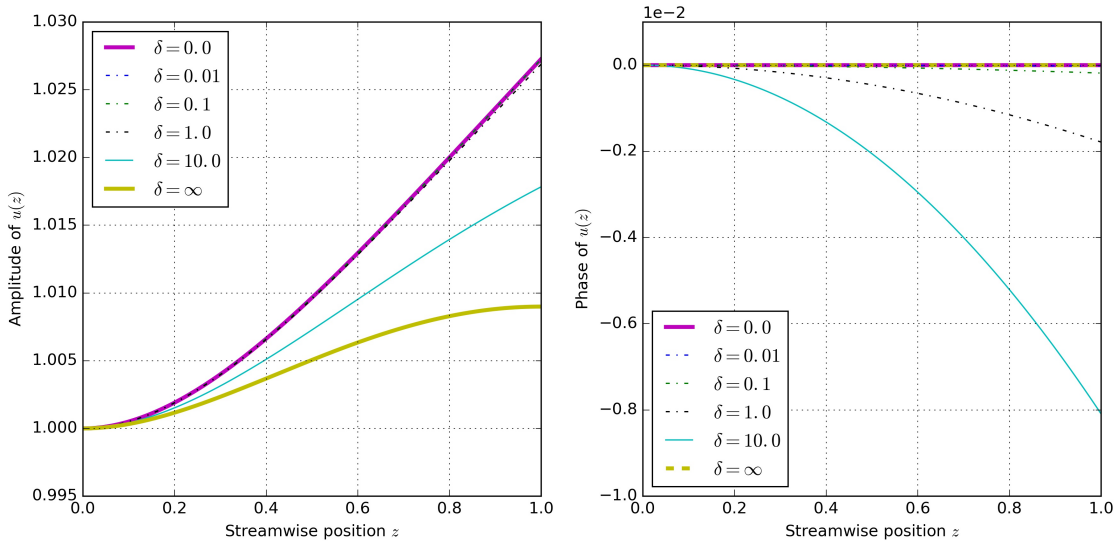

Figure 3: Amplitude and phase of the displacement function $u(z)$ for difference values of δ

When the electromechanical coupling is extremely strong, and δ is extremely large and can be seen as ∞ in mathematical sense. In this situation, the solution $u_\infty(z)$ is again real without any phase difference in the z direction. The coefficients can be analytically expressed as

$$\begin{cases} A_\infty = \dfrac{\cos\sqrt{\sigma}\sinh\sqrt{\sigma}}{\cos\sqrt{\sigma}\sinh\sqrt{\sigma}+\sin\sqrt{\sigma}\cosh\sqrt{\sigma}}, \\ B_\infty = \dfrac{\sin\sqrt{\sigma}\sinh\sqrt{\sigma}}{\cos\sqrt{\sigma}\sinh\sqrt{\sigma}+\sin\sqrt{\sigma}\cosh\sqrt{\sigma}}, \\ C_\infty = \dfrac{\sin\sqrt{\sigma}\cosh\sqrt{\sigma}}{\cos\sqrt{\sigma}\sinh\sqrt{\sigma}+\sin\sqrt{\sigma}\cosh\sqrt{\sigma}}, \\ D_\infty = \dfrac{-\sin\sqrt{\sigma}\sinh\sqrt{\sigma}}{\cos\sqrt{\sigma}\sinh\sqrt{\sigma}+\sin\sqrt{\sigma}\cosh\sqrt{\sigma}}. \end{cases} \tag{26}$$

and hence the dimensionless displacement function $u_\infty(z)$ is

$$u_\infty(z) = A_\infty\cos\sqrt{\sigma}z + B_\infty\sin\sqrt{\sigma}z + C_\infty\cosh\sqrt{\sigma}z + D_\infty\sinh\sqrt{\sigma}z - 1. \tag{27}$$

While a finite non-zero electromechanical coupling factor δ is present, which is expected in most applications, the resulting dimensionless displacement function $u(z)$ has varying magnitude and phase along the stream-wise direction or z direction. Nevertheless, it is seen from the right panel of Figure 3 that for different values of δ, the phase change of $u(z)$ is very small in the z direction, actually in the order 10^{-2}.

To make it more clear, we plot the phase of $u(z)$ at $z = 1$ versus different values of δ in Figure 4. It is clear that with the increase of δ, amplitude of the end displacement ($z = 1$) of the beam $|u(z)|$ decreases, while its phase reaches a minimum at around $\delta = 10$. This also explains the fact expressed in Figure 3 that the amplitude of displacement function $u_\delta(z)$ with $0 < \delta < \infty$ is always between that of $u_\varnothing(z)$ and $u_\infty(z)$.

As for the output voltage $V_p(t)$, output current $I_p(t)$, and output power $P_p(t)$ for the classical piezoelectric cantilever energy harvester, their corresponding complex amplitudes $\tilde{V}_p$, $\tilde{I}_p$, and $\tilde{P}_p$

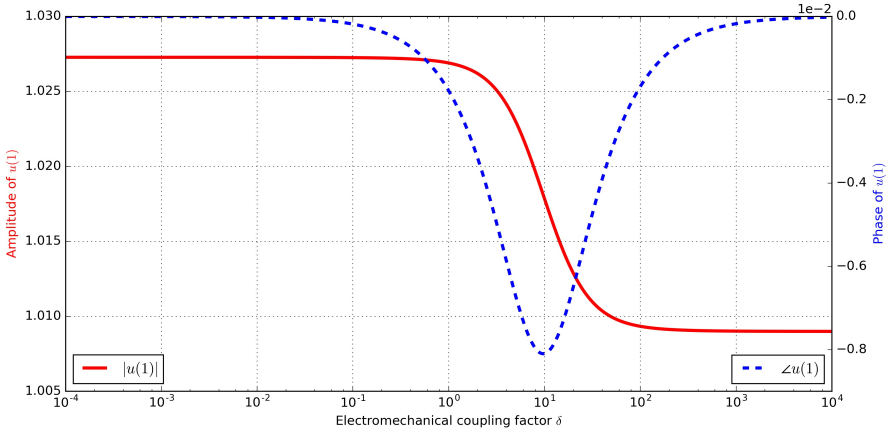

Figure 4: Amplitude and phase of the displacement function $u(z)$ at the position $z = 1$ versus electromechanical coupling factor δ.

can be formulated as

$$\begin{cases} \tilde{V}_p = -\dfrac{j\sigma\beta}{j\sigma\beta+1}\dfrac{\eta_b}{l_p}\dfrac{e_p}{C_p}u'(1), \\ \quad = -\dfrac{j\sigma\beta}{j\sigma\beta+1}\dfrac{\eta_b}{l_p}\dfrac{e_p}{C_p}\sigma^{1/2}\left(-A_\delta\sin\sqrt{\sigma}+B_\delta\cos\sqrt{\sigma}+C_\delta\sinh\sqrt{\sigma}+D_\delta\cosh\sqrt{\sigma}\right) \\ \quad = -\dfrac{j\sigma\beta}{j\sigma\beta+1}\dfrac{\eta_b}{l_p}\dfrac{e_p}{C_p}\dfrac{\sqrt{\sigma}\left(\sinh\sqrt{\sigma}-\sin\sqrt{\sigma}\right)}{1+\cos\sqrt{\sigma}\cosh\sqrt{\sigma}+\frac{j\beta\sqrt{\sigma}}{1+j\beta\sigma}\delta\left(\cos\sqrt{\sigma}\sinh\sqrt{\sigma}+\sin\sqrt{\sigma}\cosh\sqrt{\sigma}\right)} \\ \quad = -\dfrac{j\sigma\beta}{j\sigma\beta+1}\left(\dfrac{\eta_b}{l_p}\right)\left(\dfrac{e_p}{C_p}\right)\chi_p, \\ \tilde{I}_p = \tilde{V}_p/R_l = -\dfrac{j\sigma\beta}{j\sigma\beta+1}\left(\dfrac{\eta_b}{l_p}\right)\left(\dfrac{e_p}{C_pR_l}\right)\chi_p, \\ \tilde{P}_p = \tilde{V}_p^2/R_l = \left(\dfrac{\eta_b}{l_p}\right)^2\left(\dfrac{e_p}{C_p}\right)\left(\dfrac{e_p}{C_pR_l}\right)\left(\dfrac{j\sigma\beta}{j\sigma\beta+1}\right)^2\chi_p^2, \end{cases} \tag{28}$$

in which we have used the notations that

$$\chi_p = u_1'(1) = \frac{\sqrt{\sigma}\left(\sinh\sqrt{\sigma}-\sin\sqrt{\sigma}\right)}{1+\cos\sqrt{\sigma}\cosh\sqrt{\sigma}+\frac{j\beta\sqrt{\sigma}}{1+j\beta\sigma}\delta\left(\cos\sqrt{\sigma}\sinh\sqrt{\sigma}+\sin\sqrt{\sigma}\cosh\sqrt{\sigma}\right)}. \tag{29}$$

Clearly, The three output measures $\tilde{V}_p$, $\tilde{I}_p$, and $\tilde{P}_p$ are heavily dependent on another dimensionless parameter $r_d = \eta_b/l_p$. Formally, both $\tilde{V}_p$ and $\tilde{I}_p$ depend linearly upon r_d, while $\tilde{P}_p$ shows a quadratic dependence on r_d. The only dependence upon δ is introduced in χ_p. However, it should be noted that the parameter δ relies on e_p, l_p, C_p, and B_p, while the three measures $\tilde{V}_p$, $\tilde{I}_p$, and $\tilde{P}_p$ are dimensional values and depend on e_p, σ_b, and R_l. As a result, the change of parameter δ results in the change of reference voltage e_p/C_p, reference current $e_p/(C_pR_l)$, and reference power $(e_p/C_p)[e_p/(C_pR_l)]$, and therefore the corresponding values of $\tilde{V}_p$, $\tilde{I}_p$, and $\tilde{P}_p$. Hence, we may establish a bijective relation between δ and e_p, and relate the change of δ to that of e_p. In this way, we calculate the output measures at different values of δ and plot their amplitudes in Figure 5.

It is seen from Figure 5 that all the three measures show a maximum peak with the increase of δ at the approximate value of $\delta = 10$. When δ is small, or equivalently, e_p is small, amplitude of the three output measures $\tilde{V}_p$, $\tilde{I}_p$, and $\tilde{P}_p$ increase with the increase of δ. Then after the critical value of δ, a further increase of δ causes the decrease of output measures. Thus we come to a small conclusion that to obtain an optimal output performance, the electromechanical coupling factor δ should be set to an appropriate value. However, a direct calculation using the parameters introduced in the literature [17, 18] shows that the parameter δ is rather small for a typical piezoelectric cantilever energy harvester. For example, for a piezoelectric voltage constant $e_{31} = -5.35\ C/m^2$, the value of e_p is $-5.35\times10^{-5}\ C$, and the final value of δ is 0.028. According to the properties of commonly used

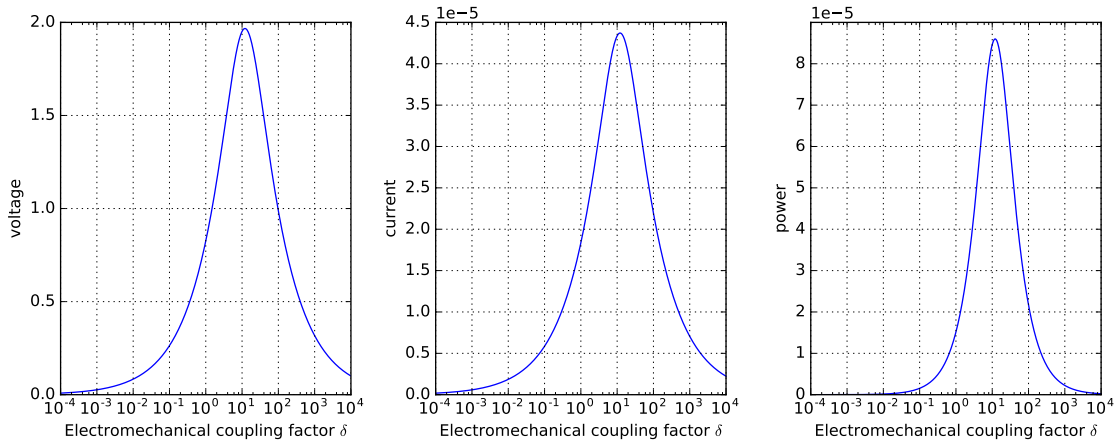

Figure 5: Voltage, current and power output for the piezoelectric cantilever energy harvester

piezoelectric materials, the parameter e_{31} is always in the range of several or several tens C/m^2 reference to be inserted. That is to say, the final value of δ can be seen always in the order of 10^{-2}, which is a rather small value according to the diagram. Hence we could present an asymptotic analysis of the performance of the classical piezoelectric energy harvester. This is the subject of the following section.

5 Asymptotic analysis of the problem

Considering that the parameter δ is small, we expand the theoretical solution to the problem in terms of the small parameter δ using the following regular expansion:

$$\begin{cases} A_\delta = A_0 + \delta A_1 + \delta^2 A_2 + \cdots, \\ B_\delta = B_0 + \delta B_1 + \delta^2 B_2 + \cdots, \\ C_\delta = C_0 + \delta C_1 + \delta^2 C_2 + \cdots, \\ D_\delta = D_0 + \delta D_1 + \delta^2 D_2 + \cdots. \end{cases} \tag{30}$$

As a result, we obtain the following successive expansion problem:
$O(\delta^0)$:

$$\begin{cases} A_0 + C_0 = 1, \\ B_0 + D_0 = 0, \\ -A_0 \cos\sqrt{\sigma} - B_0 \sin\sqrt{\sigma} + C_0 \cosh\sqrt{\sigma} + D_0 \sinh\sqrt{\sigma} = 0, \\ A_0 \sin\sqrt{\sigma} - B_0 \cos\sqrt{\sigma} + C_0 \sinh\sqrt{\sigma} + D_0 \cosh\sqrt{\sigma} = 0. \end{cases} \tag{31}$$

The solution is

$$\begin{cases} A_0 = \dfrac{1 + \cos\sqrt{\sigma}\cosh\sqrt{\sigma} - \sin\sqrt{\sigma}\sinh\sqrt{\sigma}}{2 + 2\cos\sqrt{\sigma}\cosh\sqrt{\sigma}}, \\ B_0 = \dfrac{\cosh\sqrt{\sigma}\sin\sqrt{\sigma} + \cos\sqrt{\sigma}\sinh\sqrt{\sigma}}{2 + 2\cos\sqrt{\sigma}\cosh\sqrt{\sigma}}, \\ C_0 = \dfrac{1 + \cos\sqrt{\sigma}\cosh\sqrt{\sigma} + \sin\sqrt{\sigma}\sinh\sqrt{\sigma}}{2 + 2\cos\sqrt{\sigma}\cosh\sqrt{\sigma}}, \\ D_0 = -\dfrac{\cosh\sqrt{\sigma}\sin\sqrt{\sigma} + \cos\sqrt{\sigma}\sinh\sqrt{\sigma}}{2 + 2\cos\sqrt{\sigma}\cosh\sqrt{\sigma}}. \end{cases} \tag{32}$$

Hence we have

$$-A_0 \sin\sqrt{\sigma} + B_0 \cos\sqrt{\sigma} + C_0 \sinh\sqrt{\sigma} + D_0 \cosh\sqrt{\sigma} = \frac{\sinh\sqrt{\sigma} - \sin\sqrt{\sigma}}{\cos\sqrt{\sigma}\cosh\sqrt{\sigma} + 1} \tag{33}$$

$O(\delta^1)$:

$$\begin{cases} A_1 + C_1 = 0, \\ B_1 + D_1 = 0, \\ \left(-A_1\cos\sqrt{\sigma} - B_1\sin\sqrt{\sigma} + C_1\cosh\sqrt{\sigma} + D_1\sinh\sqrt{\sigma}\right) + \\ \dfrac{j\beta\sqrt{\sigma}}{j\sigma\beta+1}\left(-A_0\sin\sqrt{\sigma} + B_0\cos\sqrt{\sigma} + C_0\sinh\sqrt{\sigma} + D_0\cosh\sqrt{\sigma}\right) = 0, \\ A_1\sin\sqrt{\sigma} - B_1\cos\sqrt{\sigma} + C_1\sinh\sqrt{\sigma} + D_1\cosh\sqrt{\sigma} = 0. \end{cases} \tag{34}$$

The solution is

$$\begin{cases} A_1 = \dfrac{j\beta\sqrt{\sigma}}{1+j\beta\sigma}\left(\dfrac{\sinh\sqrt{\sigma}-\sin\sqrt{\sigma}}{\cos\sqrt{\sigma}\cosh\sqrt{\sigma}+1}\right)\left(\dfrac{\cos\sqrt{\sigma}+\cosh\sqrt{\sigma}}{2\cos\sqrt{\sigma}\cosh\sqrt{\sigma}+2}\right) \\ B_1 = \dfrac{j\beta\sqrt{\sigma}}{1+j\beta\sigma}\left(\dfrac{\sinh\sqrt{\sigma}-\sin\sqrt{\sigma}}{\cos\sqrt{\sigma}\cosh\sqrt{\sigma}+1}\right)\left(\dfrac{-\sinh\sqrt{\sigma}+\sin\sqrt{\sigma}}{2\cos\sqrt{\sigma}\cosh\sqrt{\sigma}+2}\right) \\ C_1 = \dfrac{j\beta\sqrt{\sigma}}{1+j\beta\sigma}\left(\dfrac{\sinh\sqrt{\sigma}-\sin\sqrt{\sigma}}{\cos\sqrt{\sigma}\cosh\sqrt{\sigma}+1}\right)\left(-\dfrac{\cos\sqrt{\sigma}+\cosh\sqrt{\sigma}}{2\cos\sqrt{\sigma}\cosh\sqrt{\sigma}+2}\right) \\ D_1 = \dfrac{j\beta\sqrt{\sigma}}{1+j\beta\sigma}\left(\dfrac{\sinh\sqrt{\sigma}-\sin\sqrt{\sigma}}{\cos\sqrt{\sigma}\cosh\sqrt{\sigma}+1}\right)\left(\dfrac{-\sin\sqrt{\sigma}+\sinh\sqrt{\sigma}}{2\cos\sqrt{\sigma}\cosh\sqrt{\sigma}+2}\right) \end{cases} \tag{35}$$

Then we have

$$\begin{aligned} &-A_1\sin\sqrt{\sigma} + B_1\cos\sqrt{\sigma} + C_1\sinh\sqrt{\sigma} + D_1\cosh\sqrt{\sigma} \\ &= \frac{j\beta\sqrt{\sigma}}{1+j\beta\sigma}\left(\frac{\sin\sqrt{\sigma}-\sinh\sqrt{\sigma}}{\cos\sqrt{\sigma}\cosh\sqrt{\sigma}+1}\right)\left(\frac{\cos\sqrt{\sigma}\sinh\sqrt{\sigma}+\sin\sqrt{\sigma}\cosh\sqrt{\sigma}}{\cos\sqrt{\sigma}\cosh\sqrt{\sigma}+1}\right) \end{aligned} \tag{36}$$

$O(\delta^2)$:

$$\begin{cases} A_2 + C_2 = 0, \\ B_2 + D_2 = 0, \\ \left(-A_2\cos\sqrt{\sigma} - B_2\sin\sqrt{\sigma} + C_2\cosh\sqrt{\sigma} + D_2\sinh\sqrt{\sigma}\right) + \\ \dfrac{j\beta\sqrt{\sigma}}{j\sigma\beta+1}\left(-A_1\sin\sqrt{\sigma} + B_1\cos\sqrt{\sigma} + C_1\sinh\sqrt{\sigma} + D_1\cosh\sqrt{\sigma}\right) = 0, \\ A_2\sin\sqrt{\sigma} - B_2\cos\sqrt{\sigma} + C_2\sinh\sqrt{\sigma} + D_2\cosh\sqrt{\sigma} = 0. \end{cases} \tag{37}$$

The solution is

$$\begin{cases} A_2 = \left(\dfrac{j\beta\sqrt{\sigma}}{1+j\beta\sigma}\right)^2\left(\dfrac{\sinh\sqrt{\sigma}-\sin\sqrt{\sigma}}{\cos\sqrt{\sigma}\cosh\sqrt{\sigma}+1}\right)\left(\dfrac{\cos\sqrt{\sigma}\sinh\sqrt{\sigma}+\sin\sqrt{\sigma}\cosh\sqrt{\sigma}}{\cos\sqrt{\sigma}\cosh\sqrt{\sigma}+1}\right)\left(\dfrac{\cos\sqrt{\sigma}+\cosh\sqrt{\sigma}}{2\cos\sqrt{\sigma}\cosh\sqrt{\sigma}+2}\right) \\ B_2 = \left(\dfrac{j\beta\sqrt{\sigma}}{1+j\beta\sigma}\right)^2\left(\dfrac{\sinh\sqrt{\sigma}-\sin\sqrt{\sigma}}{\cos\sqrt{\sigma}\cosh\sqrt{\sigma}+1}\right)\left(\dfrac{\cos\sqrt{\sigma}\sinh\sqrt{\sigma}+\sin\sqrt{\sigma}\cosh\sqrt{\sigma}}{\cos\sqrt{\sigma}\cosh\sqrt{\sigma}+1}\right)\left(\dfrac{-\sinh\sqrt{\sigma}+\sin\sqrt{\sigma}}{2\cos\sqrt{\sigma}\cosh\sqrt{\sigma}+2}\right) \\ C_2 = \left(\dfrac{j\beta\sqrt{\sigma}}{1+j\beta\sigma}\right)^2\left(\dfrac{\sinh\sqrt{\sigma}-\sin\sqrt{\sigma}}{\cos\sqrt{\sigma}\cosh\sqrt{\sigma}+1}\right)\left(\dfrac{\cos\sqrt{\sigma}\sinh\sqrt{\sigma}+\sin\sqrt{\sigma}\cosh\sqrt{\sigma}}{\cos\sqrt{\sigma}\cosh\sqrt{\sigma}+1}\right)\left(-\dfrac{\cos\sqrt{\sigma}+\cosh\sqrt{\sigma}}{2\cos\sqrt{\sigma}\cosh\sqrt{\sigma}+2}\right) \\ D_2 = \left(\dfrac{j\beta\sqrt{\sigma}}{1+j\beta\sigma}\right)^2\left(\dfrac{\sinh\sqrt{\sigma}-\sin\sqrt{\sigma}}{\cos\sqrt{\sigma}\cosh\sqrt{\sigma}+1}\right)\left(\dfrac{\cos\sqrt{\sigma}\sinh\sqrt{\sigma}+\sin\sqrt{\sigma}\cosh\sqrt{\sigma}}{\cos\sqrt{\sigma}\cosh\sqrt{\sigma}+1}\right)\left(\dfrac{-\sin\sqrt{\sigma}+\sinh\sqrt{\sigma}}{2\cos\sqrt{\sigma}\cosh\sqrt{\sigma}+2}\right) \end{cases} \tag{38}$$

Indeed, we can continue to obtain the coefficients for higher order (≥ 2) expansions, as shown in the appendices (To add some comments) using successive iteration method. Nevertheless, it suffices here to consider up to the second order expansion $u^{(0)}(z)$, $u^{(1)}(z)$, and $u^{(2)}(z)$, respectively:

$$\begin{cases} u^{(0)}(z) = u_0(z), \\ u^{(1)}(z) = u_0(z) + \delta u_1(z), \\ u^{(2)}(z) = u_0(z) + \delta u_1(z) + \delta^2 u_2(z), \end{cases} \tag{39}$$

where the terms $u_0(z)$, $u_1(z)$, and $u_2(z)$ are defined as

$$\begin{cases} u_0(z) = A_0\cos\sqrt{\sigma}z + B_0\sin\sqrt{\sigma}z + C_0\cosh\sqrt{\sigma}z + D_0\sinh\sqrt{\sigma}z - 1, \\ u_1(z) = A_1\cos\sqrt{\sigma}z + B_1\sin\sqrt{\sigma}z + C_1\cosh\sqrt{\sigma}z + D_1\sinh\sqrt{\sigma}z, \\ u_2(z) = A_2\cos\sqrt{\sigma}z + B_2\sin\sqrt{\sigma}z + C_2\cosh\sqrt{\sigma}z + D_2\sinh\sqrt{\sigma}z. \end{cases} \tag{40}$$

For different values of δ and σ (Here in this simulation, the value of σ is changed through the variance of base excitation frequency f_b), the asymptotic approximations of the dimensionless relative beam displacement function $u(z;\delta)$ up to the second order $u^{(0)}(z)$, $u^{(1)}(z)$, and $u^{(2)}(z)$ are calculated and compared to the closed solution $u(z;\delta)$ itself. The results are shown in Figure 6, 7, 8, 9, 10, 11, 12.

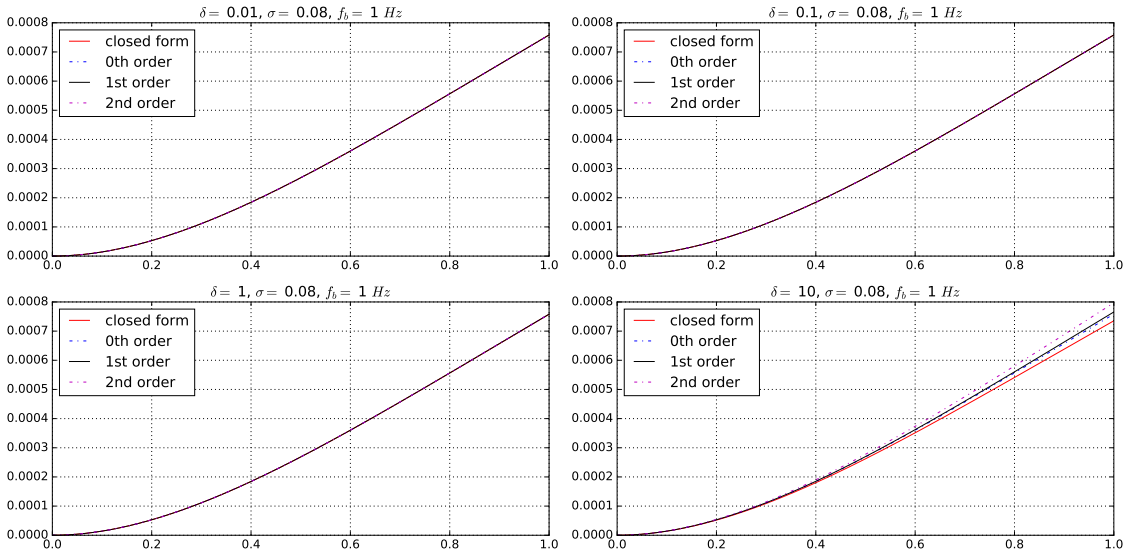

Figure 6: Comparison for the different orders of asymptotic expansion for the dimensionless relative displacement function $u_\delta(z)$.

Notice from Figure 2 that the first mode resonant frequency for the device is around 45 Hz. It is seen from these results that a smaller value of δ results in a better approximation, whatever the value of f_b. This is consistent with the philosophy behind asymptotic expansion. Besides, for the frequency away from the resonant frequency, the approximation results are relatively accurate in the range of $\delta \leq 0.1$ depending on the value of f_b. While when the base excitation frequency f_b is close to a resonance, for example $f_b = 45\ Hz$, the approximation results are not accurate even at the value of $\delta = 0.01$. That is to say, the asymptotic expansion in terms of δ is not uniform with respect to parameter σ. Especially, the existence of resonance actually restrict the behavior of the asymptotic expansion. Around the resonance the expansion will show low accuracy, while away from the resonance, the expansion accuracy is easily retained. Nonetheless, for commonly used piezoelectric materials and energy harvesting device configuration, the value of δ is usually in the range of 10^{-2}. Hence, it is generally validated to use the asymptotic expansion method to approximate the dimensionless displacement function $u(z;\delta)$. Furthermore, in view of the approximating performances of the asymptotic expansions to different orders, it suffices to keep only the $0th$ order terms. Then, we have that

$$u(z;\delta) \approx u^{(0)}(z) = A_0 \cos\sqrt{\sigma}z + B_0 \sin\sqrt{\sigma}z + C_0 \cosh\sqrt{\sigma}z + D_0 \sinh\sqrt{\sigma}z - 1. \tag{41}$$

This is exactly the displacement function of a pure elastic cantilever beam. It means that for most piezoelectric energy harvesting devices, due to the fact that the electromechanical coupling factor is relatively small, the displacement function is not much affected. In this way, we have indeed uncoupled the electrical part and elastic part of a piezoelectric energy harvesting device. It should be noted that the approximation is not valid near the resonant points.

Theoretically, the first order derivative of the dimensionless relative displacement function $u(z;\delta)$ is

$$u'(z;\delta) = \sigma^{1/2}\left(-A_\delta \sin\sqrt{\sigma}z + B_\delta \cos\sqrt{\sigma}z + C_\delta \sinh\sqrt{\sigma}z + D_\delta \cosh\sqrt{\sigma}z\right). \tag{42}$$

$$\chi_p = u_1'(1) = \frac{\sqrt{\sigma}\left(\sinh\sqrt{\sigma} - \sin\sqrt{\sigma}\right)}{1 + \cos\sqrt{\sigma}\cosh\sqrt{\sigma} + \frac{j\beta\sqrt{\sigma}}{1+j\beta\sigma}\delta\left(\cos\sqrt{\sigma}\sinh\sqrt{\sigma} + \sin\sqrt{\sigma}\cosh\sqrt{\sigma}\right)}. \tag{43}$$

The value of this function at the free end ($z = 1$) is just the output index χ_p according to equation (29). To see the influences of δ and f_b, therefore σ, upon χ_p, we firstly calculate the values of χ_p

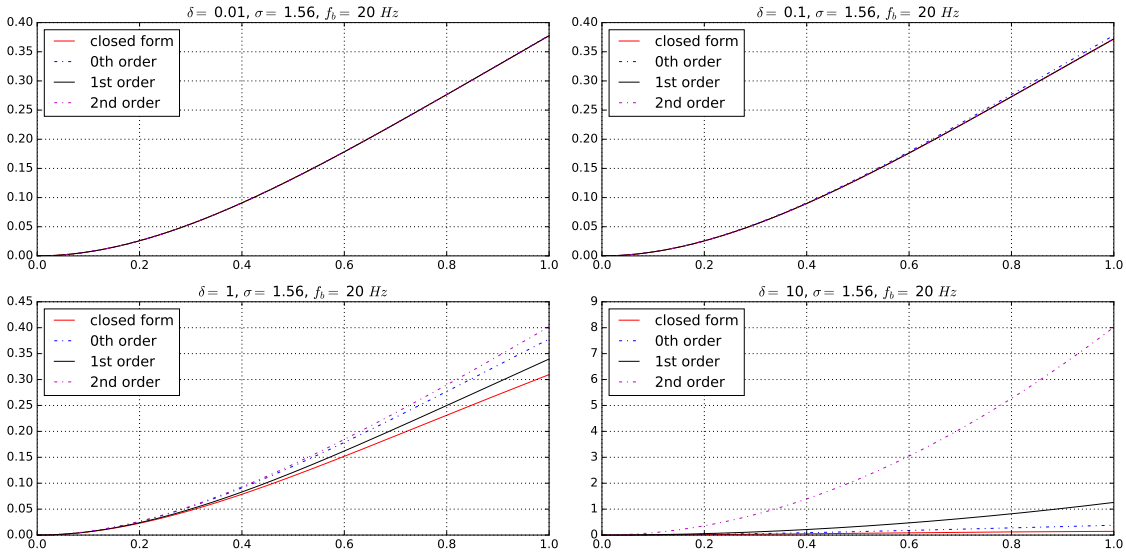

Figure 7: Comparison for the different orders of asymptotic expansion for the dimensionless relative displacement function $u_\delta(z)$.

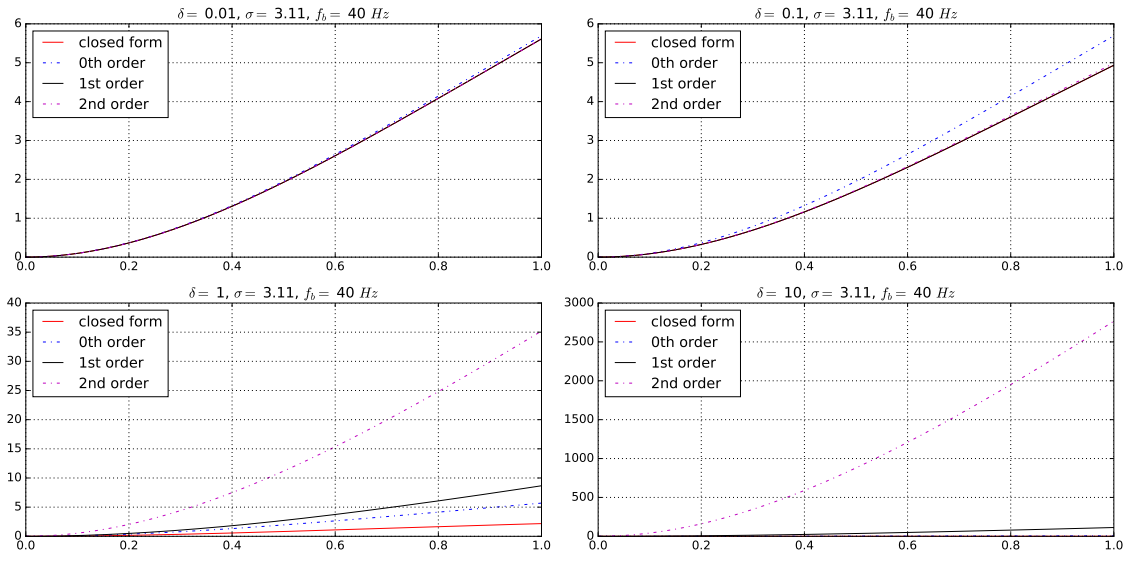

Figure 8: Comparison for the different orders of asymptotic expansion for the dimensionless relative displacement function $u_\delta(z)$.

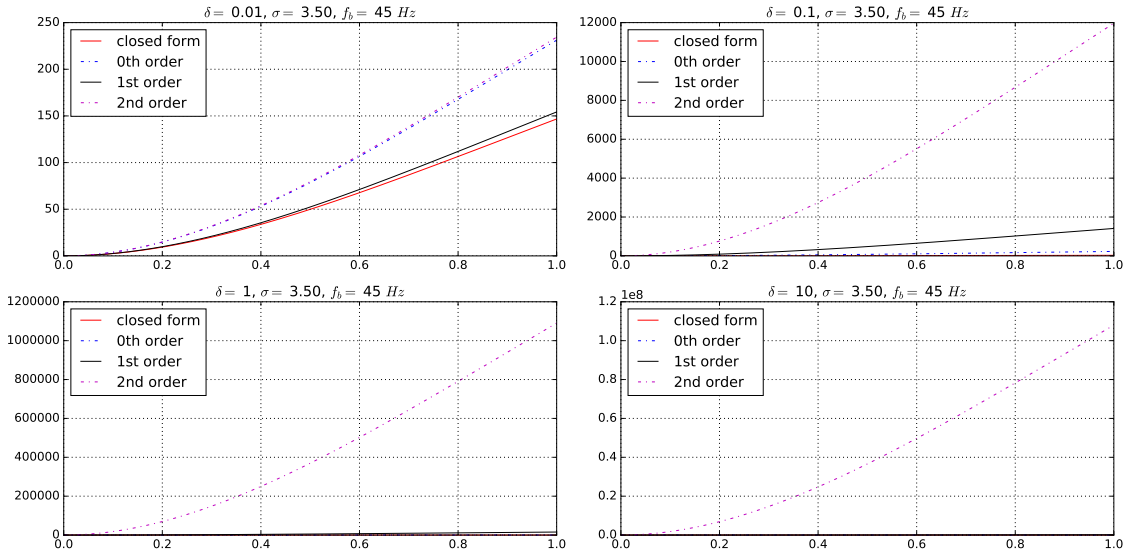

Figure 9: Comparison for the different orders of asymptotic expansion for the dimensionless relative displacement function $u_\delta(z)$.

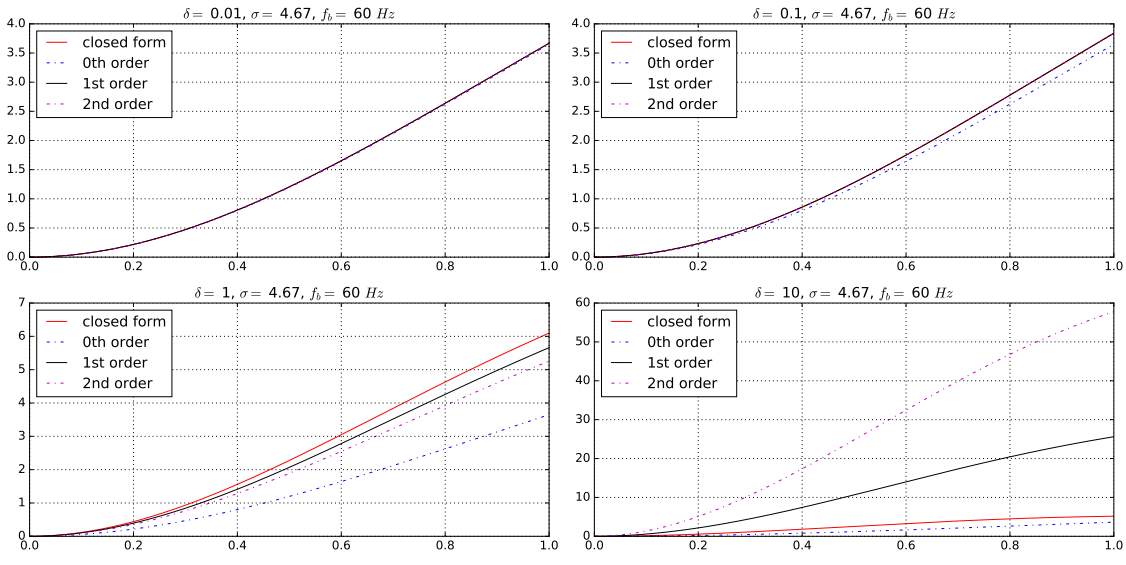

Figure 10: Comparison for the different orders of asymptotic expansion for the dimensionless relative displacement function $u_\delta(z)$.

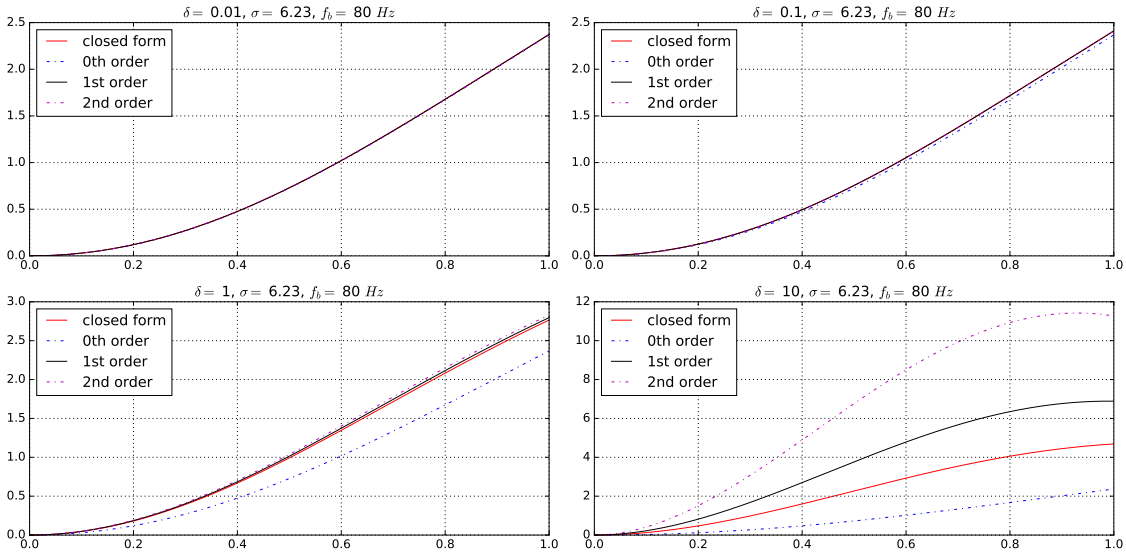

Figure 11: Comparison for the different orders of asymptotic expansion for the dimensionless relative displacement function $u_\delta(z)$.

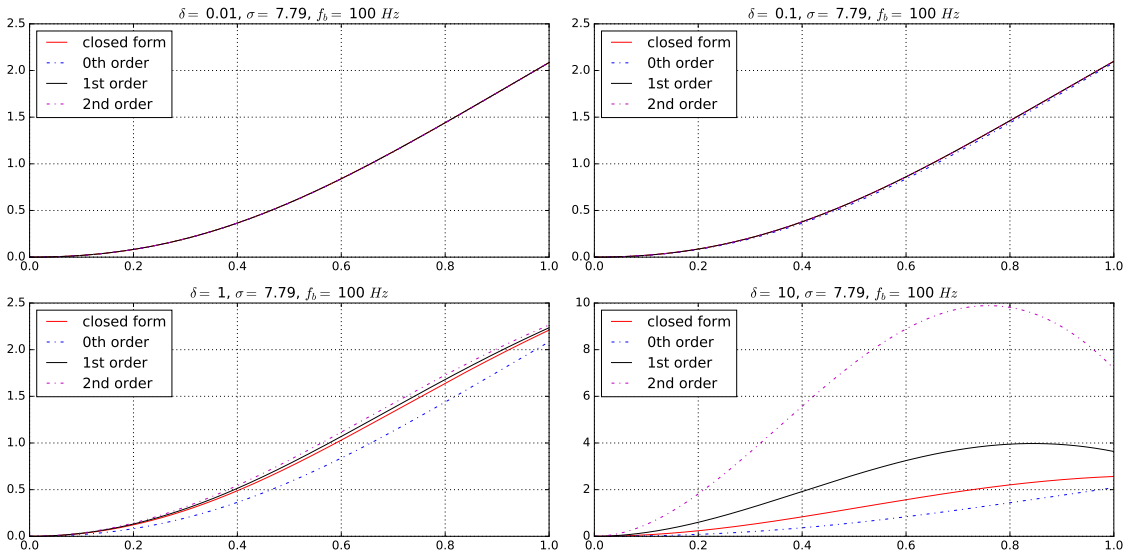

Figure 12: Comparison for the different orders of asymptotic expansion for the dimensionless relative displacement function $u_\delta(z)$.

for different values of δ by fixing the value of f_b to be some discrete values. The results are shown in Figure 13.

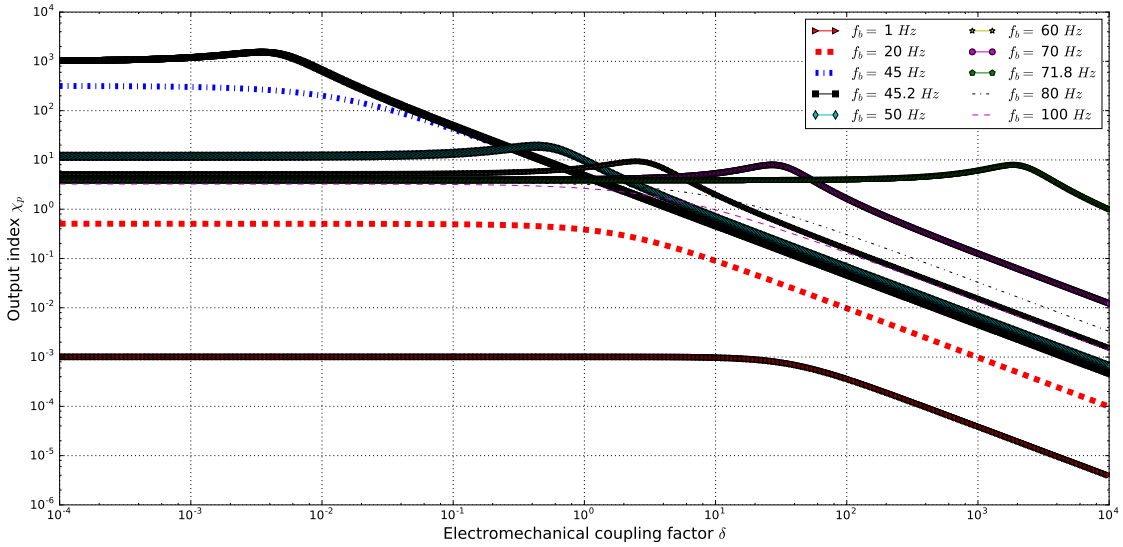

Figure 13: Output index χ_p as a function of electromechanical coupling factor δ at different values of base excitation frequency f_b.

It is seen that the dependence of χ_p upon δ shows two different modes in the frequency range of $1 - 100\ Hz$. For the frequencies of $45.2\ Hz \leq f_b \leq 71.8\ Hz$, a peak corresponding to a critical value of δ_p is present in the considered range of δ. When δ is smaller than δ_p, the output index χ_p increases along with δ, and when δ is larger than δ_p, the output index χ_p decreases with the increase of δ. On the other hand, for the frequency range of $f_b \leq 45\ Hz$ or $f_b \geq 80\ Hz$, the output index χ_p shows a monotonic decrease with respect to the increase δ.

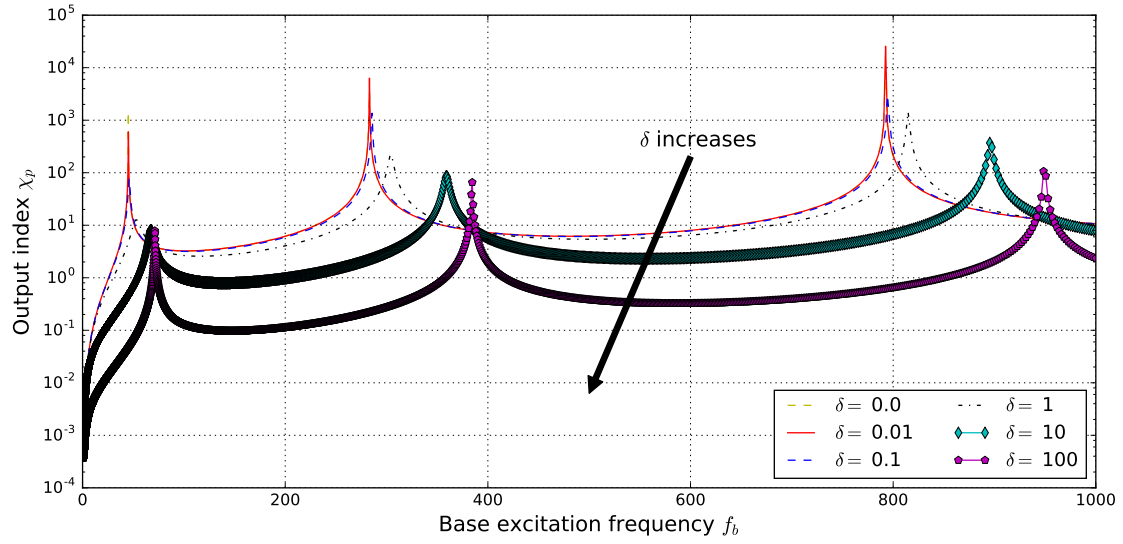

Figure 14: Output index χ_p as a function of base excitation frequency f_b at different values of electromechanical coupling factor δ.

Alternatively, by fixing the values of δ to a discrete set of numbers, we calculate the values of χ_p in relation to different values of f_b. This is very similar to a frequency response of the output index as a function of σ. The results are shown in Figure 14. It is clearly shown that with the increase of electromechanical coupling factor δ, the resonant frequencies to the system increase with the increase of δ. This is clearly shown in the shift to the right of the frequency response curve.

Besides, we add in this figure the case where $\delta = 0.0$ as a reference. Simple comparisons show that the discrepancy between the frequency response curves related to the case of $\delta = 0$, $\delta = 0.01$, and $\delta = 0.1$ is small. A direct conclusion is that for relatively small values of electromechanical coupling factor δ, the output index χ_p can be approximated by

$$\chi_p \approx \frac{\sqrt{\sigma}\left(\sinh\sqrt{\sigma} - \sin\sqrt{\sigma}\right)}{1 + \cos\sqrt{\sigma}\cosh\sqrt{\sigma}}. \tag{44}$$

As a result, the output performance measures $\tilde{V}_p$, $\tilde{I}_p$, and $\tilde{P}_p$ can be approximated by

$$\begin{cases} \tilde{V}_p = -\dfrac{j\sigma\beta}{j\sigma\beta + 1}\left(\dfrac{\eta_b}{l_p}\right)\left(\dfrac{e_p}{C_p}\right)\chi_p, \\ \quad = -\dfrac{j\sigma\beta}{j\sigma\beta + 1}\left(\dfrac{\eta_b}{l_p}\right)\left(\dfrac{e_p}{C_p}\right)\dfrac{\sqrt{\sigma}\left(\sinh\sqrt{\sigma} - \sin\sqrt{\sigma}\right)}{1 + \cos\sqrt{\sigma}\cosh\sqrt{\sigma}}, \\ \tilde{I}_p = \tilde{V}_p/R_l = -\dfrac{j\sigma\beta}{j\sigma\beta + 1}\left(\dfrac{\eta_b}{l_p}\right)\left(\dfrac{e_p}{C_pR_l}\right)\chi_p, \\ \quad = -\dfrac{j\sigma\beta}{j\sigma\beta + 1}\left(\dfrac{\eta_b}{l_p}\right)\left(\dfrac{e_p}{C_pR_l}\right)\dfrac{\sqrt{\sigma}\left(\sinh\sqrt{\sigma} - \sin\sqrt{\sigma}\right)}{1 + \cos\sqrt{\sigma}\cosh\sqrt{\sigma}}, \\ \tilde{P}_p = \tilde{V}_p^2/R_l = \left(\dfrac{\eta_b}{l_p}\right)^2\left(\dfrac{e_p}{C_p}\right)\left(\dfrac{e_p}{C_pR_l}\right)\left(\dfrac{j\sigma\beta}{j\sigma\beta + 1}\right)^2\chi_p^2, \\ \quad = \left(\dfrac{\eta_b}{l_p}\right)^2\left(\dfrac{e_p}{C_p}\right)\left(\dfrac{e_p}{C_pR_l}\right)\left(\dfrac{j\sigma\beta}{j\sigma\beta + 1}\right)^2\left(\dfrac{\sqrt{\sigma}\left(\sinh\sqrt{\sigma} - \sin\sqrt{\sigma}\right)}{1 + \cos\sqrt{\sigma}\cosh\sqrt{\sigma}}\right)^2. \end{cases} \tag{45}$$

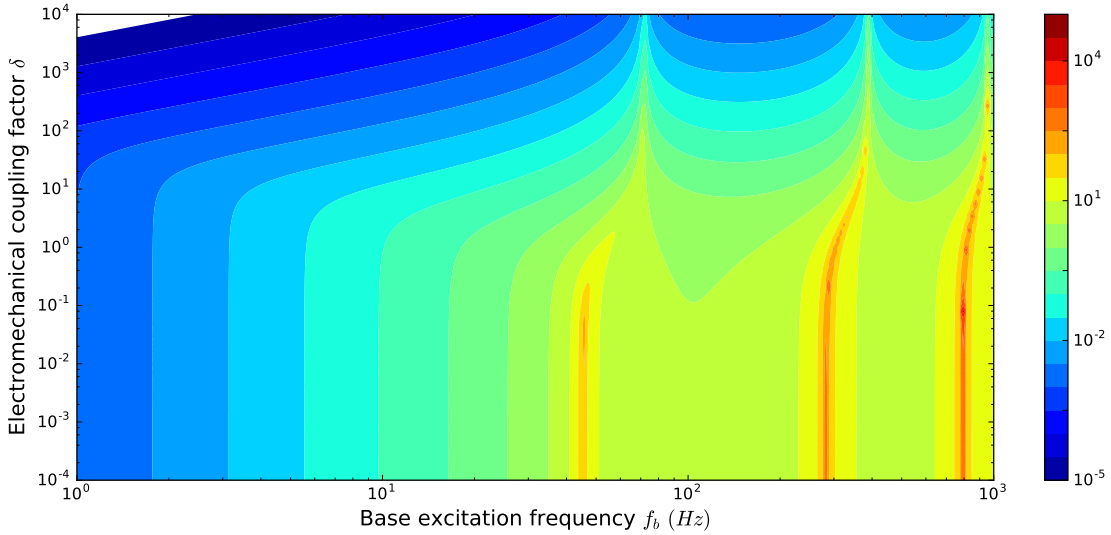

Figure 15: Output index χ_p as a function of base excitation frequency f_b and electromechanical coupling factor δ.

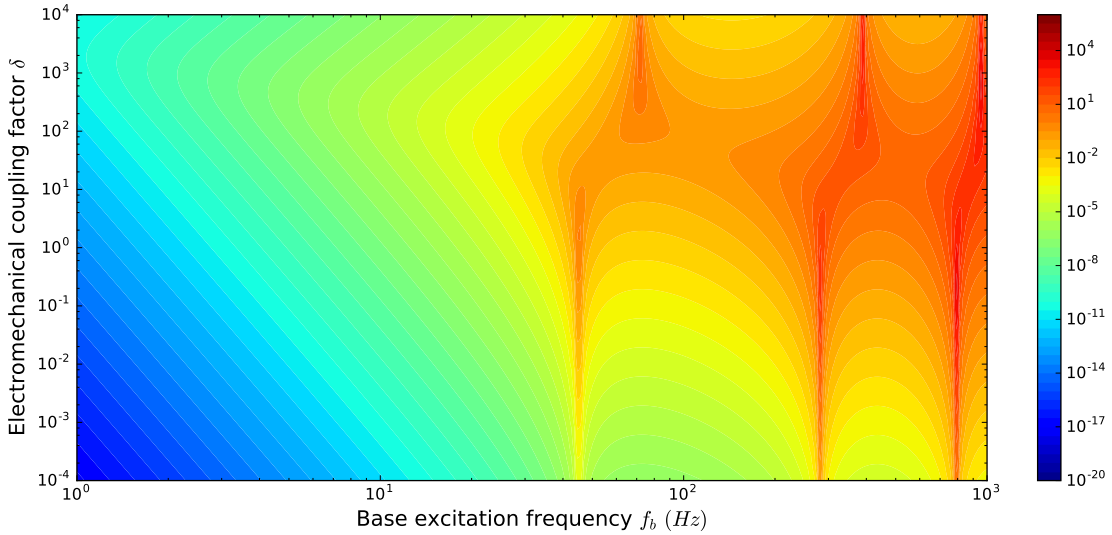

Figure 16: Output voltage $\tilde{V}_p$ as a function of base excitation frequency f_b and electromechanical coupling factor δ.

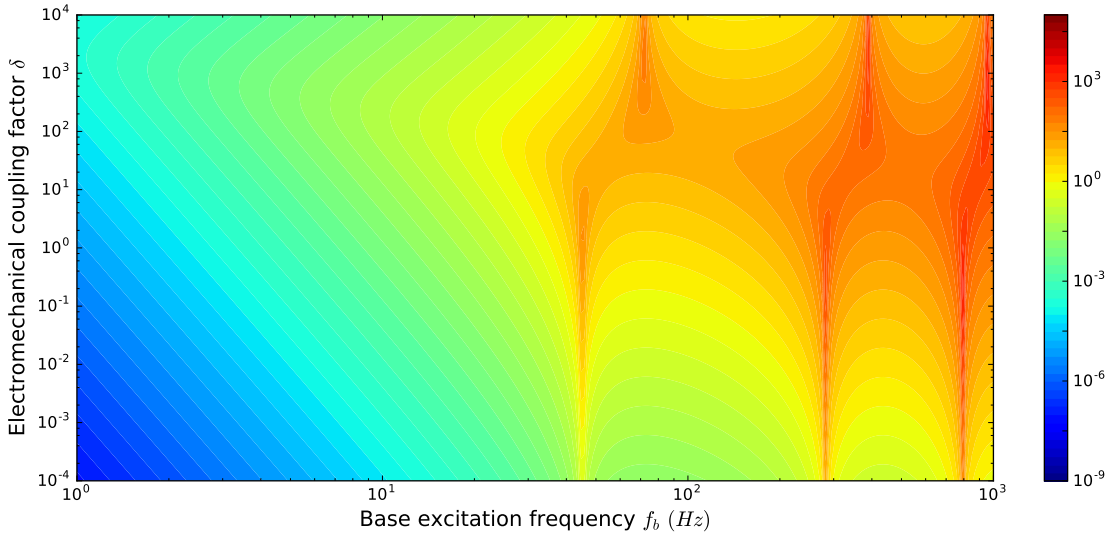

Figure 17: Output voltage $\tilde{P}_p$ as a function of base excitation frequency f_b and electromechanical coupling factor δ.

6 Conclusion

Appendices

The asymptotic expansion of equation (23) can be found using an iterative method. In fact, for higher order expansions ($k \geq 1$), we have the following iterative relation:

$$\begin{cases} A_{k+1} + C_{k+1} = 0, \\ B_{k+1} + D_{k+1} = 0, \\ \left(-A_{k+1}\cos\sqrt{\sigma} - B_{k+1}\sin\sqrt{\sigma} + C_{k+1}\cosh\sqrt{\sigma} + D_{k+1}\sinh\sqrt{\sigma}\right) + \\ \dfrac{j\beta\sqrt{\sigma}}{j\sigma\beta+1}\left(-A_k\sin\sqrt{\sigma} + B_k\cos\sqrt{\sigma} + C_k\sinh\sqrt{\sigma} + D_k\cosh\sqrt{\sigma}\right) = 0, \\ A_{k+1}\sin\sqrt{\sigma} - B_{k+1}\cos\sqrt{\sigma} + C_{k+1}\sinh\sqrt{\sigma} + D_{k+1}\cosh\sqrt{\sigma} = 0, \end{cases} \tag{46}$$

whose solution is expressed by

$$\begin{cases} A_{k+1} = \left(\dfrac{j\beta\sqrt{\sigma}}{1+j\beta\sigma}\right)\left(\dfrac{\cos\sqrt{\sigma}+\cosh\sqrt{\sigma}}{2\cos\sqrt{\sigma}\cosh\sqrt{\sigma}+2}\right)(Q_k), \\ B_{k+1} = \left(\dfrac{j\beta\sqrt{\sigma}}{1+j\beta\sigma}\right)\left(\dfrac{-\sinh\sqrt{\sigma}+\sin\sqrt{\sigma}}{2\cos\sqrt{\sigma}\cosh\sqrt{\sigma}+2}\right)(Q_k), \\ C_{k+1} = \left(\dfrac{j\beta\sqrt{\sigma}}{1+j\beta\sigma}\right)\left(-\dfrac{\cos\sqrt{\sigma}+\cosh\sqrt{\sigma}}{2\cos\sqrt{\sigma}\cosh\sqrt{\sigma}+2}\right)(Q_k), \\ D_{k+1} = \left(\dfrac{j\beta\sqrt{\sigma}}{1+j\beta\sigma}\right)\left(\dfrac{-\sin\sqrt{\sigma}+\sinh\sqrt{\sigma}}{2\cos\sqrt{\sigma}\cosh\sqrt{\sigma}+2}\right)(Q_k), \end{cases} \tag{47}$$

in which

$$Q_k = -A_k\sin\sqrt{\sigma} + B_k\cos\sqrt{\sigma} + C_k\sinh\sqrt{\sigma} + D_k\cosh\sqrt{\sigma}. \tag{48}$$

In terms of Q_k ($k \geq 0$), we have the following iterative relation

$$Q_{k+1} = -\left(\frac{\sin\sqrt{\sigma}\cosh\sqrt{\sigma}+\cos\sqrt{\sigma}\sinh\sqrt{\sigma}}{\cos\sqrt{\sigma}\cosh\sqrt{\sigma}+1}\right)\left(\frac{j\beta\sqrt{\sigma}}{1+j\beta\sigma}\right)Q_k, \tag{49}$$

and the initial two values Q_0 and Q_1:

$$\begin{cases} Q_0 = \dfrac{\sinh\sqrt{\sigma}-\sin\sqrt{\sigma}}{\cos\sqrt{\sigma}\cosh\sqrt{\sigma}+1}, \\ Q_1 = \dfrac{j\beta\sqrt{\sigma}}{1+j\beta\sigma}\left(\dfrac{\sin\sqrt{\sigma}-\sinh\sqrt{\sigma}}{\cos\sqrt{\sigma}\cosh\sqrt{\sigma}+1}\right)\left(\dfrac{\cos\sqrt{\sigma}\sinh\sqrt{\sigma}+\sin\sqrt{\sigma}\cosh\sqrt{\sigma}}{\cos\sqrt{\sigma}\cosh\sqrt{\sigma}+1}\right). \end{cases} \tag{50}$$

Hence it is shown that for $k \geq 0$,

$$Q_k = \left[-\left(\frac{j\beta\sqrt{\sigma}}{1+j\beta\sigma}\right)\left(\frac{\sin\sqrt{\sigma}\cosh\sqrt{\sigma}+\cos\sqrt{\sigma}\sinh\sqrt{\sigma}}{\cos\sqrt{\sigma}\cosh\sqrt{\sigma}+1}\right)\right]^k\left(\frac{\sinh\sqrt{\sigma}-\sin\sqrt{\sigma}}{\cos\sqrt{\sigma}\cosh\sqrt{\sigma}+1}\right). \tag{51}$$

As a result, we obtain that for $k \geq 1$,

$$\begin{cases} A_k = \left(\dfrac{j\beta\sqrt{\sigma}}{1+j\beta\sigma}\right)^k\left(\dfrac{-\sin\sqrt{\sigma}\cosh\sqrt{\sigma}-\cos\sqrt{\sigma}\sinh\sqrt{\sigma}}{\cos\sqrt{\sigma}\cosh\sqrt{\sigma}+1}\right)^{k-1}\left(\dfrac{\sinh\sqrt{\sigma}-\sin\sqrt{\sigma}}{\cos\sqrt{\sigma}\cosh\sqrt{\sigma}+1}\right)\left(\dfrac{\cos\sqrt{\sigma}+\cosh\sqrt{\sigma}}{2\cos\sqrt{\sigma}\cosh\sqrt{\sigma}+2}\right), \\ B_k = \left(\dfrac{j\beta\sqrt{\sigma}}{1+j\beta\sigma}\right)^k\left(\dfrac{-\sin\sqrt{\sigma}\cosh\sqrt{\sigma}-\cos\sqrt{\sigma}\sinh\sqrt{\sigma}}{\cos\sqrt{\sigma}\cosh\sqrt{\sigma}+1}\right)^{k-1}\left(\dfrac{\sinh\sqrt{\sigma}-\sin\sqrt{\sigma}}{\cos\sqrt{\sigma}\cosh\sqrt{\sigma}+1}\right)\left(\dfrac{-\sinh\sqrt{\sigma}+\sin\sqrt{\sigma}}{2\cos\sqrt{\sigma}\cosh\sqrt{\sigma}+2}\right), \\ C_k = \left(\dfrac{j\beta\sqrt{\sigma}}{1+j\beta\sigma}\right)^k\left(\dfrac{-\sin\sqrt{\sigma}\cosh\sqrt{\sigma}-\cos\sqrt{\sigma}\sinh\sqrt{\sigma}}{\cos\sqrt{\sigma}\cosh\sqrt{\sigma}+1}\right)^{k-1}\left(\dfrac{\sinh\sqrt{\sigma}-\sin\sqrt{\sigma}}{\cos\sqrt{\sigma}\cosh\sqrt{\sigma}+1}\right)\left(\dfrac{-\cos\sqrt{\sigma}-\cosh\sqrt{\sigma}}{2\cos\sqrt{\sigma}\cosh\sqrt{\sigma}+2}\right), \\ D_k = \left(\dfrac{j\beta\sqrt{\sigma}}{1+j\beta\sigma}\right)^k\left(\dfrac{-\sin\sqrt{\sigma}\cosh\sqrt{\sigma}-\cos\sqrt{\sigma}\sinh\sqrt{\sigma}}{\cos\sqrt{\sigma}\cosh\sqrt{\sigma}+1}\right)^{k-1}\left(\dfrac{\sinh\sqrt{\sigma}-\sin\sqrt{\sigma}}{\cos\sqrt{\sigma}\cosh\sqrt{\sigma}+1}\right)\left(\dfrac{-\sin\sqrt{\sigma}+\sinh\sqrt{\sigma}}{2\cos\sqrt{\sigma}\cosh\sqrt{\sigma}+2}\right). \end{cases}$$

Acknowledgements

References

[1] Beeby SP, Tudor MJ, White N. Energy harvesting vibration sources for microsystems applications. Measurement science and technology. 2006;17(12):R175.

[2] Anton SR, Sodano HA. A review of power harvesting using piezoelectric materials (2003–2006). Smart materials and Structures. 2007;16(3):R1.

[3] Zhou M, Al-Furjan MSH, Zou J, Liu W. A review on heat and mechanical energy harvesting from human–Principles, prototypes and perspectives. Renewable and Sustainable Energy Reviews. 2018;82:3582–3609.

[4] Safaei M, Sodano HA, Anton SR. A review of energy harvesting using piezoelectric materials: state-of-the-art a decade later (2008–2018). Smart Materials and Structures. 2019;28(11):113001.

[5] Roundy S, Wright PK, Rabaey J. A study of low level vibrations as a power source for wireless sensor nodes. Computer communications. 2003;26(11):1131–1144.

[6] Dutoit NE, Wardle BL, Kim SG. Design considerations for MEMS-scale piezoelectric mechanical vibration energy harvesters. Integrated ferroelectrics. 2005;71(1):121–160.

[7] Stephen NG. On energy harvesting from ambient vibration. Journal of sound and vibration. 2006;293(1-2):409–425.

[8] Cottone F, Vocca H, Gammaitoni L. Nonlinear energy harvesting. Physical Review Letters. 2009;102(8):080601.

[9] Erturk A, Inman DJ. On mechanical modeling of cantilevered piezoelectric vibration energy harvesters. Journal of intelligent material systems and structures. 2008;19(11):1311–1325.

[10] Crandall SH. Dynamics of mechanical and electromechanical systems. McGraw-Hill; 1968.

[11] Hagood NW, Chung WH, Von Flotow A. Modelling of piezoelectric actuator dynamics for active structural control. Journal of intelligent material systems and structures. 1990;1(3):327–354.

[12] Sodano HA, Park G, Inman D. Estimation of electric charge output for piezoelectric energy harvesting. Strain. 2004;40(2):49–58.

[13] Lu F, Lee H, Lim S. Modeling and analysis of micro piezoelectric power generators for micro-electromechanical-systems applications. Smart Materials and Structures. 2003;13(1):57.

[14] Chen SN, Wang GJ, Chien MC. Analytical modeling of piezoelectric vibration-induced micro power generator. Mechatronics. 2006;16(7):379–387.

[15] Ajitsaria J, Choe SY, Shen D, Kim D. Modeling and analysis of a bimorph piezoelectric cantilever beam for voltage generation. Smart Materials and Structures. 2007;16(2):447.

[16] Kreyszig E. Introductory functional analysis with applications. vol. 1. wiley New York; 1978.

[17] Erturk A, Inman DJ. A distributed parameter electromechanical model for cantilevered piezoelectric energy harvesters. Journal of vibration and acoustics. 2008;130(4):041002.

[18] Erturk A, Inman DJ. An experimentally validated bimorph cantilever model for piezoelectric energy harvesting from base excitations. Smart materials and structures. 2009;18(2):025009.

[19] Erturk A, Tarazaga PA, Farmer JR, Inman DJ. Effect of strain nodes and electrode configuration on piezoelectric energy harvesting from cantilevered beams. Journal of Vibration and Acoustics. 2009;131(1):011010.